A simplified time stepping nonlinear mesh based reluctance network for machine design

M. Hage Hassan, *Student Member, IEEE,* G. Krebs, C. Marchand, *Member, IEEE*

***Abstract*— This paper presents a quick and reliable methodology for machine designing. The methodology is based on reluctance network and applied to design three phase axial flux machines. The modeled reluctance network allows taking into account nonlinear operating conditions. It is solved by computing meshes' magnetic flux and the network topology is updated for each rotor position. Therefore, a number of steady state steps are considered to simulate machine's rotation. At first the modeling methodology is presented. The models are validated in linear and nonlinear mode by means of a 2D finite element software, experimental validation of a machine is presented, and finally the sizing of the machines on a driving cycle in linear mode is carried out.**

***Index Terms*— Design methodology, design optimization, Nonlinear systems, Permanent magnet machines, Automotive applications.**

I. INTRODUCTION

IN electrical machine modeling, magnetic equivalent circuit (MEC) based on reluctance network (RelNet) method is known to be a good compromise between computation time and precision. It can take into account material's non linearity, the rotor position [1] and local losses. The reluctance network approach uses the magnetoelectric analogy where reluctances replace resistances. Three types of reluctances are described. Time dependent, these are the reluctances that vary with the saturation, air gap reluctances that vary with the rotor position and constant reluctances describing flux leakage and permanent magnet if present.

In this paper the modeled machines are Axial Flux Machines (AFM). The choice of modeling this type of machines for electrical vehicles is due to some of their distinct advantages [2-3] over Radial Flux Machines (RFM). They can be designed to have a higher power to weight ratio resulting in higher efficiency, as well as that they are smaller in size than the RFM and have disc shaped rotor and stator. Although these machines have the ability to have multiple discs [4] and can be founded in multiple topologies. Here is presented the modeling of two different topologies. The first one concerns a 6-teeth 4-poles and 6-teeth and 8-poles torus machines Fig.1. These machines are composed by two rotors and one stator. The third structure, see Fig.2, is a 12-teeth 10-poles machine, with two stators and one rotor.

Due to confidential issues this machine will not be revealed in details in terms of modeling and dimensions.

M. Hage Hassan, G. Krebs, C. Marchand, are with Laboratoire de Génie Electrique de Paris (LGEP), CNRS UMR 8507; SUPELEC; Université Pierre et Marie Curie P6; Université Paris-Sud; 11 rue Joliot Curie, Plateau de Moulon, 91192 Gif sur Yvette CEDEX, FRANCE. (E-mail: Maya.Hage-Hassan@lgep.supelec.fr).

II. MODELING METHODOLOGY

The global reluctance network system can be solved by computing the nodal magnetic potential [5] where the incidence matrix describing the connection between reluctances relies on vertices and edges, or by computing the meshes magnetic flux [6] where the incidence matrix describes the connection between meshes and edges.

Although mesh based equivalent circuits did not receive much attention, as opposed to nodal formulation, a recent comparison between both models [7], shows the advantage to use a mesh-based model, under nonlinear operating conditions.

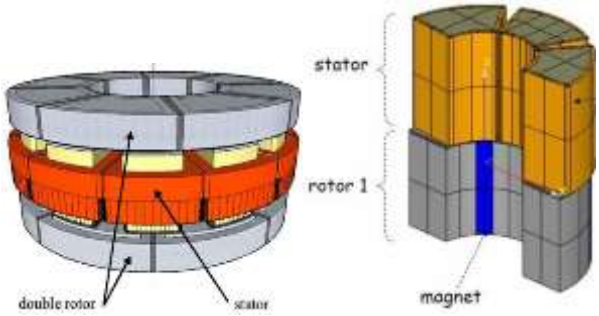

Fig. 1. Torus axial flux machine double rotor/single stator [8]

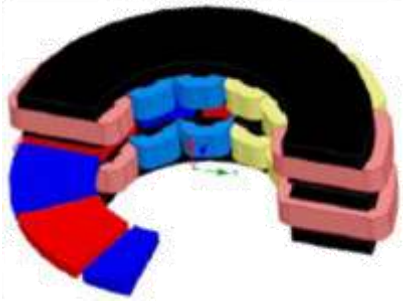

Fig. 2. Axial flux machine double stator/single rotor

In nodal formulation, the deduced Jacobian can be ill conditioned. Therefore the convergence of Newton-Raphson algorithm cannot be assured or can be characterized by a large number of iterations on the opposite of the mesh based model. Other advantage described in [9], shows the influence of the B-H curve in promoting a lower iteration count and improving convergence rate in case of mesh analysis.

Hereby, is developed a simplified mesh based magnetic equivalent circuit (MEC) in order to model two three phase axial flux machines. The first machine is a 6-teeth 4-poles structure and the second one 6-teeth and 8-poles. The basis of the MEC formalism relies on works appeared in [6] and [10]. These works propose the development of mesh based equivalent circuit formalism permitting to simplify the

automatic generation of system describing the network.

A. Mesh based resolution method

Describing the magnetic equivalent circuit returns to state, the active element as the magnetomotive forces (MMF) sources and the passive elements as the flux tubes (reluctances). Reluctances are described by their geometrical shape, magnetic nature and the settled relation between them, which in other terms mean the description of magnetic field circulation.

The last point can be exploited by means of incidence matrices. Incidence matrices allow us to build the relation between vertices and edges of a directed graph [11]. In case of magnetic circuit, magnetic potential and oriented flux are assigned respectively at each vertex (v) and edge (e). Another type of matrix can take place, which is a structure matrix that describes the relation between chosen oriented flux meshes and corresponding flux edges. Though, starting from the incidence vertices-edges matrix [A] the number of *m* independent meshes can be determined through Euler's formula for connected graph, such that; *m=e-v+1*. A meshes-edges matrix [S] describing the structure can be established [6]. The next step is to assign for each edge its corresponding reluctance. For linear behavior the reluctances describing magnetic material is given as in (1).

$$R = \left(\frac{1}{\mu}\right)\left(\frac{L}{Section}\right) \tag{1}$$

When taking into account the magnetic materials saturation, the reluctances are given by (2). The reluctance is expressed in terms of the corresponding edge magnetic flux Φ and the magnetic field *H*.

$$R = \left(\mathrm{H}\left(\frac{\Phi}{Section}\right).Section \Big/ \Phi\right)\left(\frac{L}{Section}\right) \tag{2}$$

In order to model the axial flux machines, a 2D equivalent linear modeling Fig.3 is proposed [8]. The figure on the left represents the active surface of the axial machine. Its equivalent representation (right figure) is possible using the root mean square radius given in (3) as the equivalent radius and the active equivalent length and depth calculated as in (4).

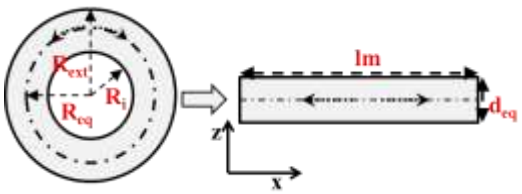

Fig. 3. 2D equivalent linearization

$$R_{eq} = \sqrt{\left(R_{ext}{}^2 + R_i{}^2\right)/2} \tag{3}$$

$$lm = 2\pi R_{eq},\ d_{eq} = \left(R_{ext}{}^2 - R_i{}^2\right)\Big/\left(2R_{eq}\right) \tag{4}$$

As a result of this linearization the 2D linear model of the axial flux machine is given in Fig. 4 where half part of the 6-teeth 8-poles machine is represented.

For this reason, the chosen approximation form for reluctances is a parallelepiped one. One should note that the simplification made in regard to reluctance form, will affect the final result accuracy, but as it will be discussed later on it is not in the heart of the global formalism. In both expressions (1) (2), geometrical parameters appear independently of the materials magnetic state. Thus these parameters can be handled to the equations to be solved separately and adapted to the chosen machine's geometry.

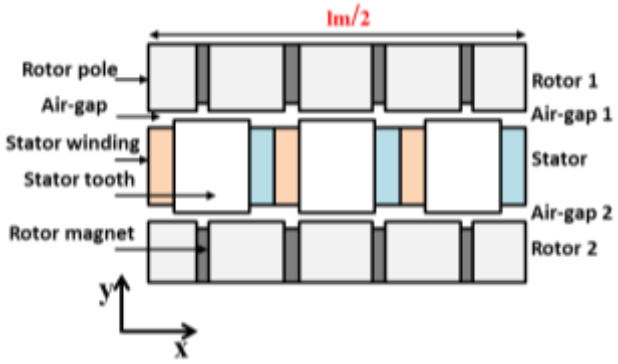

Fig. 4. 2D equivalent model of 2D 6-teeth 8-poles axial machine

B. Rotor and stator reluctances

In our modeling strategy, the use of a reluctance network does not aim in replacing finite element model, but to establish a reliable simplified one. For this reason, the reluctances describing the machines are simplified. Due to geometrical and magnetic symmetries, only a quarter part of both machines needs to be modeled.

For the rotor parts; the pole, half yoke and magnet are represented each by a single reluctance; *Rp*, *Ry*, *Rm* Fig. 5. As for the stator Fig. 6, half of a tooth is modeled and represented by one reluctance *Rt*, as well as flux leakage between teeth *Rl*. Reluctances values are computed using (1) or (2). In order to take into account periodic condition, two loops must be defined: a loop including leakage flux reluctances *Rl* for the stator as for the rotor the loop includes yoke and magnet reluctances.

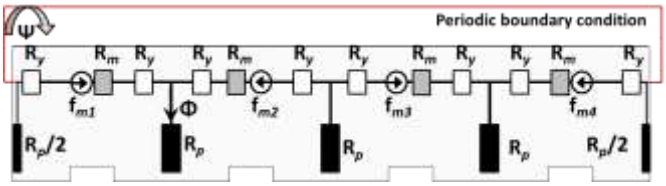

Fig.5. RelNet circuit for the rotor

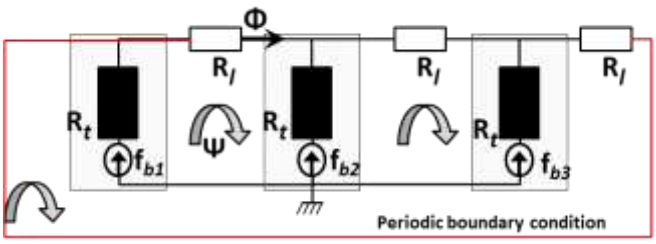

Fig. 6. RelNet circuit for half of the stator

A particular attention is given to the air-gap area, as it is the essence when considering the rotor displacement.

C. Reluctance network of the airgap

The network describing the air gap must take into account the movement of the rotor relative to the stator. For this reason, the air-gap is modeled by three layers of reluctances Fig.7.

Horizontal reluctances (a_x): Is the central layer. The number of reluctances describing it depends on the chosen discretization step along active length as in Table. I. This layer will act as an intermediate between the rotor and the stator as well as the base to connect the vertical reluctances.

Vertical reluctances (a_y): Two layers are defined. The fixed layer is anchored to the stator and to the horizontal air-gap layer. The moving layer describes the junction between rotor and the air-gap. The number of these vertical reluctances depends on step discretization of rotor poles. To take into account periodic conditions, a loop must be defined at the central layer. The discretization step dx is determined by means of (5). The machine's RelNet is given in Figure. 8.

$$dx = (lm/p)/360 \tag{5}$$

TABLE I
MACHINES AIR-GAP DISCRETIZATION

Machine	lm/2	Discretization dx	a_x
6/4	352 (mm)	$1.95e^{-3}$(mm)	180
6/8	352 (mm)	$0.9778e^{-3}$(mm)	352

The chosen discretization step for stator tooth and rotor pole is the same as dx. The air-gap width e is set to 0.5 mm, thus the horizontal and vertical reluctances are given by (6).

$$a_x = dx/(\mu_0.e.d_{eq}),\ a_y = (e/2)/(\mu_0.dx.d_{eq}) \tag{6}$$

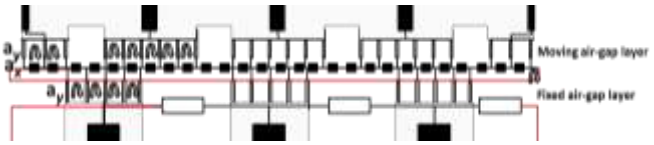

Fig. 7. Air-gap RelNet

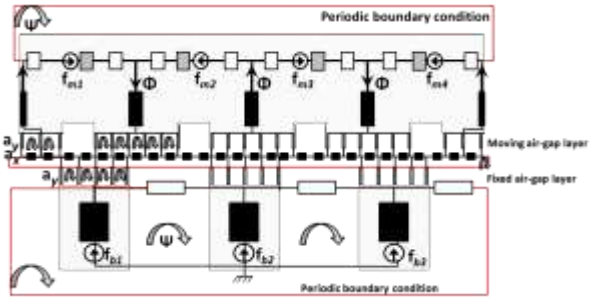

Fig. 8. RelNet for the 6-teeth 8poles machine

D. Computing Formalisms

At first, incidences matrices must be built in terms of vertices-edges. Matrix elements are determined as in (7), whereas meshes-edges matrix elements are defined as in (8).

$$a_{ij}\begin{cases} +1 & edge\ j\ starts\ from\ vertice\ i \\ -1 & edge\ j\ ends\ at\ vertice\ i \\ 0 & vertice\ i\ is\ not\ an\ extremity\ to\ edge\ j \end{cases} \tag{7}$$

$$s_{ij}\begin{cases} +1 & if\ \ branche\ j \in M_i^{+} \\ -1 & if\ \ branche\ j \in M_i^{-} \\ 0 & if\ \ branche\ j \notin M_i^{+} \cup M_i^{-} \end{cases} \tag{8}$$

In nodal formulation the equation to be solved is (9), where [P] is a diagonal matrix containing permeances describing all edges. The system variables are the magnetic potential (V). F_{mm} are the magnetomotive forces in other terms the present sources. Edges' fluxes Φ are computed through (10).

$$[\mathbf{A}]^{T}[\mathbf{P}][\mathbf{A}](\mathbf{V}) - [\mathbf{A}]^{T}[\mathbf{P}](F_{mm}) = 0 \tag{9}$$

$$\Phi = [\mathbf{P}][\mathbf{A}](\mathbf{V}) - [\mathbf{P}](F_{mm}) \tag{10}$$

E. Nonlinear modeling

With the purpose of determining outputs values of a machine, i.e. torque (T), Electromotive forces (Emf), magnetic forces (F_n, F_t), energies (W). It is important at first sight to determine magnetic flux circulating in the machine. For the chosen model it has to be supplied by three-phase alternative currents. A machine's map in terms of magnetic flux is established for all reluctances. It is function of *nb* rotor position, *nc* current values and *np* phase angle values. From this 4D flux matrix, mean Torque and Emf coefficients maps Fig.9, Fig.10, are deduced as a function of *nc* current values and *np* phase shift values. Though in saturation mode, the map is established as follows:

Step 1; establish incidence matrix [S], describing reluctance network connections at current rotor position.

Step 2; calculate magnetomotive forces for all edges given by f_{mm}= [f^{ag}_x, f^{ag}_{yr}, f^{rot}, f^{ag}_{yf},f^{stat}].

Stator magnetomotive forces are given by f^{stat}= [$F_{b1,}$ $F_{b2,}$ F_{b3}] for the current and phase angle values. The magnetomotive forces for meshes F_{mm}=[S].f_{mm}.

Step 3; resolve the linear system (11) to determine meshes' fluxes in linear mode Ψ:

$$(F_{mm}) - [\mathbf{S}][\mathbf{R}][\mathbf{S}]^{T}(\Psi^{L}) = 0 \tag{11}$$

Step 4; initialize Newton-Raphson algorithm such that: $\Psi^{NL}{}_0 = \Psi^{L}$.

Step 5; solve nonlinear system (12) using (13). [Cg] is the diagonal matrix describing reluctances' length; H magnetic field described by (16), (Section) the vector describing reluctances sections as for [Dsection] it is the diagonal matrix describing reluctances' sections.

$$f(\Psi) = (F_{mm}) - [\mathbf{S}][\mathbf{C_g}]H([\mathbf{S}]^{T}\Psi^{NL}Section^{-1}) = 0 \tag{12}$$

$$\text{Newton-Raphson: } \Psi_{k+1}{}^{NL} = \Psi_k{}^{NL} - \lambda.J(\Psi_k{}^{NL})^{-1}.f(\Psi_k{}^{NL}) \tag{13}$$

The jacobien is given by (15)

$$J(\Psi) = -[\mathbf{S}][\mathbf{C_g}]\left[\frac{d\,H([\mathbf{S}]^{T}\Psi^{NL}Section^{-1})}{d\Psi}\right][\mathbf{Dsection}][\mathbf{S}]^{T} \tag{14}$$

Step 6; compute branches flux $\Phi^{NL}{}_{nijk}$=$[S]^{T}\Psi^{NL}{}_{nijk}$ (15)

One should note that in order to resolve the presented systems (9-15), matrices are not inverted, we transformed

matrices to sparse ones and computed variables by means of cholesky factorized matrices.

TABLE II
COMPUTATION TIME FOR ONE OPERATING POINT

Machine	Model	Elements number	Steps number	Time
6/4	Linear	555	60	1.5 s
6/4	Non linear	555	60	30 s
6/8	Linear	1078	45	7 s
6/8	Non linear	1078	45	130 s

Analytical equation (16) is used to describe the B-H curve Fig.11, [12].

$$H(B) = k_1.B^{k_2} + k_5.B^{k_6}\frac{e^{(B-k_3)^{k_4}}}{1+e^{(B-k_3)^{k_4}}} \qquad (16)$$

The used coefficients in Table. III describe the M40050A metal sheets [13].

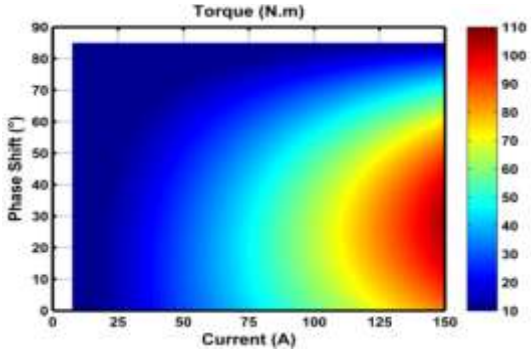

Fig. 9. Mean torque map

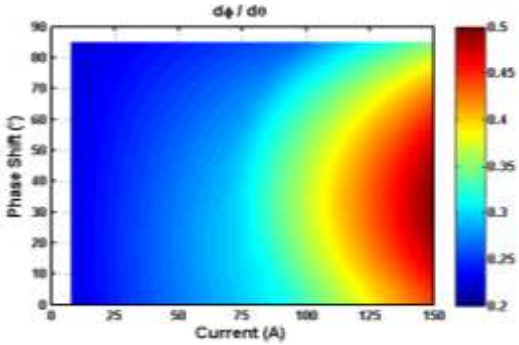

Fig. 10. Max flux derivative map

TABLE III
B-H CURVE COEFFICIENTS

Metal sheet	k_1	k_2	k_3	k_4	k_5	k_6
M40050A	112.85	0.54	1.87	5.74	1051.8	6.03

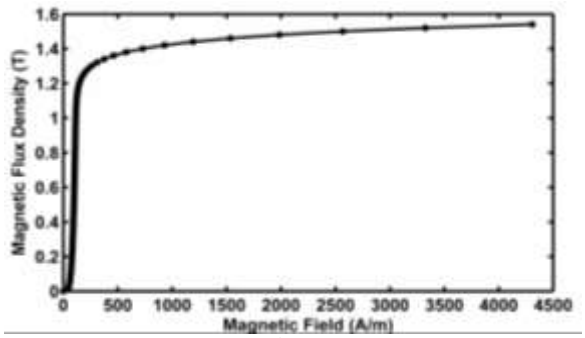

Fig. 11. B-H curve for M40050A metal sheets

III. VALIDATION WITH 2D FINITE ELEMENT MODELING

In order to validate the MEC model, hereby presented a comparison between waveforms of phase linkage flux, flux derivative, deduced from FEA and RelNet under linear Fig.12-13 and non linear conditions Fig.14-15 for the 6/8 machine. In order, to calculate the Emf the used formula is given by (17), where the first term represent the flux derivative and the second the speed in rad.s^{-1}.

$$Emf = \frac{\partial \Phi}{\partial \theta}\frac{\partial \theta}{\partial t} \qquad (17)$$

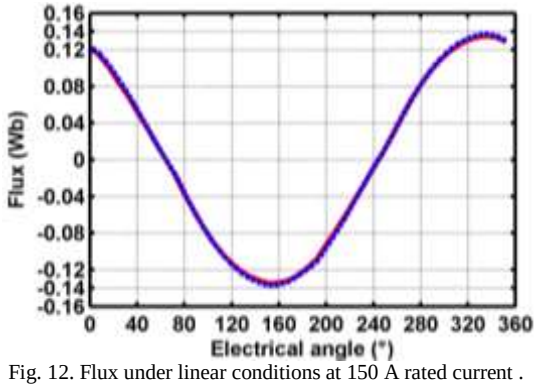

Fig. 12. Flux under linear conditions at 150 A rated current . Dashed line-RelNet. Continuous line-2D.FEA

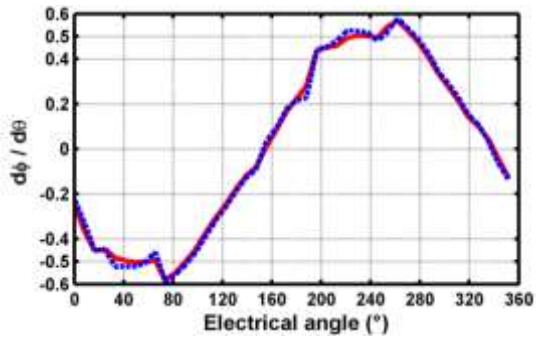

Fig. 13. Flux derivative under linear conditions at 150 A rated current . Dashed line-RelNet. Continuous line-2D.FEA

Under non linear conditions a horizontal shift appears this shifting results from the simplified hypothesis taken on the level of rotor reluctances. In order to reduce this shifting rotor magnets must be discretized by several reluctances which may increases computation time and lead to a model close to the FE model.

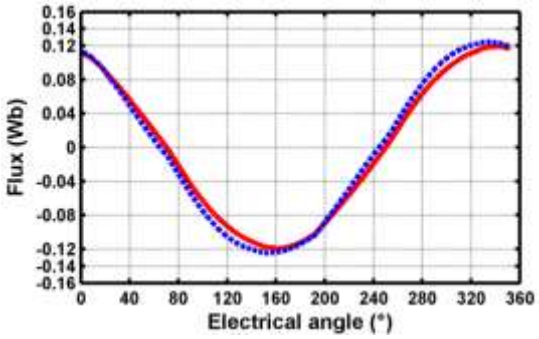

Fig. 14. Flux under non linear conditions at 150 A rated current . Dashed line-RelNet. Continuous line-2D.FEA

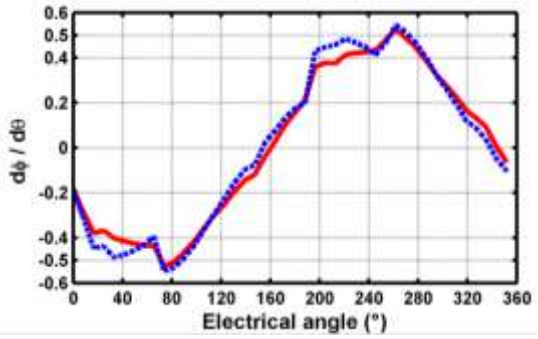

Fig. 15. Flux derivative under non linear conditions at 150 A rated current. Dashed line-RelNet. Continuous line-2D.FEA

F. Cogging torque

Cogging torque and torque ripple can be determined through Co-Energy (E) calculation or by means of Maxwell stress Tensor. The disadvantage of using the Energy method is the simulation time, where this method requires the determination of ΔE between two instances.

In the proposed modeling strategy, the air-gap is discretized on three levels, from the horizontal reluctances one can deduce the tangential magnetic field (H_t), as for the normal magnetic flux density (B_n) it can be calculated by means of the vertical moving layer reluctances. Taking into account the ability to calculate these two variables, cogging torque can be calculated using Maxwell stress tensor (18)

$$\begin{cases} \vec{F}_n = \left(\dfrac{B_n^2}{2\mu} - \dfrac{\mu H_t^2}{2} \right).\vec{n} \\ \vec{F}_t = B_n.\vec{H}_t \end{cases} \tag{18}$$

Torque created by means of F_t through (19), where C represents a closed circuit defined in the air-gap.

$$\Gamma = R_{eq}.d_{eq} \oint_C B_n.H_t \tag{19}$$

A comparison between normal flux density deduced from FEA and RelNet, see Fig.16, shows the good accordance between both curves and highlights the powerful utility of the proposed air-gap reluctances distribution.

As for the torque ripple, hereby a comparison between FEA and RelNet under linear conditions Fig.17 and non linear conditions Fig.18 at 150 A rated current. Both models gave the same mean torque value, the torque curves in linear and non linear conditions shows good accordance between FE model and RelNet model.

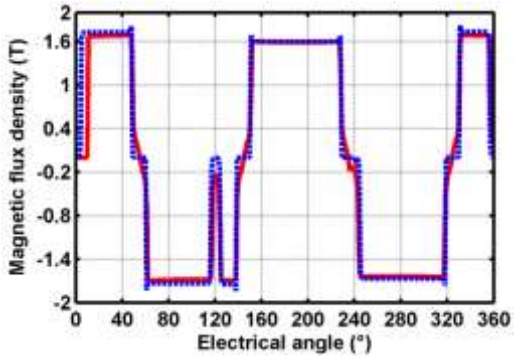

Fig. 16. No load normal flux density (B_n) . Dashed line-RelNet. Continuous line-2D.FEA

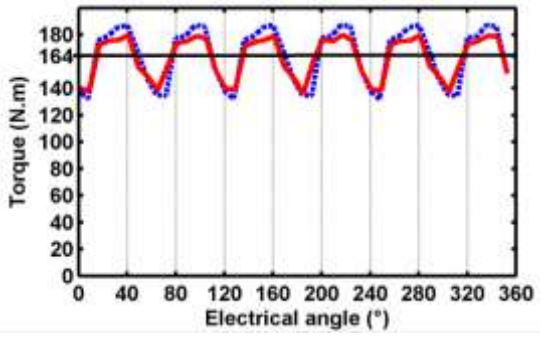

Fig. 17. Torque ripple under linear conditions at 150 A rated current. Dashed line-RelNet. Continuous line-2D.FEA

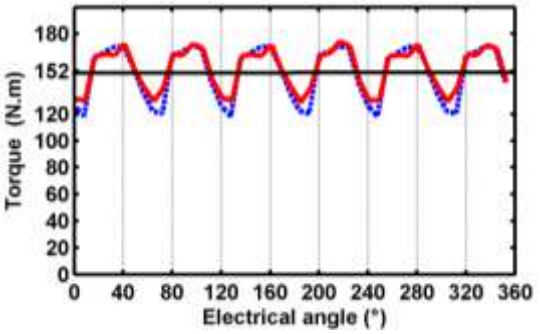

Fig. 18. Torque ripple under non linear conditions at 150 A rated current. Dashed line-RelNet. Continuous line-2D.FEA.

IV. EXPERIMENTAL VALIDATION

In order to validate our predimensioning modeling strategy, experimental results are needed. For the lake of time to produce a machine and put in place a bench test, we proceeded to the modeling of an existing axial flux machine of a different topology; double stator of 12 teeth and a single rotor with 10 poles, where the magnets are inserted in a nonmagnetic material, on the opposite of our modeled first axial flux machines. A comparison between these two topologies is given in Fig. 19, [14].

The model was as well compared to a model developed on FEMM and validated under linear and non linear conditions. In Fig. 20 is presented a comparison between RelNet model and experimental results for the phase-to-phase voltage at 52(rad.s^{-1}).

The sinusoidal curves progression compared between RelNet and experimental results are satisfactory. The RelNet model gives a good prediction of the results to expect. As for numerical results, the phase-to-phase calculated using RelNet model is equal to 60 (V) while the experimental one it's at 65 (V) which gives us 8% of error.

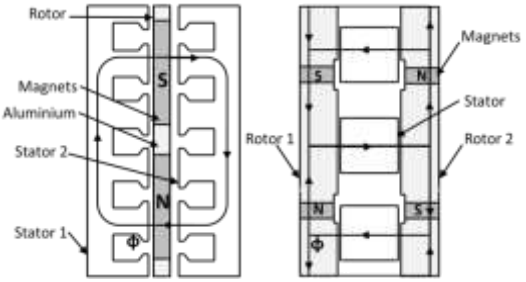

Fig. 19. On the left: Double stator/ single rotor IPM axial flux machine. On the right: Double rotor/single stator IPM axial flux machine.

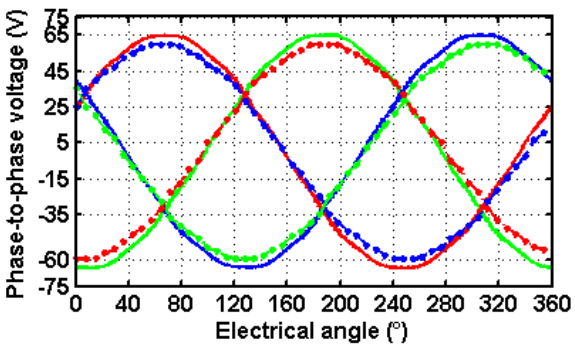

Fig. 20. Phase-to-Phase Voltage. Dotted lines-RelNet model. Continuous lines-Experimental results

Under 110 (A) rated current, the machine provides a torque of 216 (N.m). Using the RelNet model the deduced torque is 213 (N.m) Fig. 21. Generally, the theoretical torque is superior to the experimental one, in our case due to the 2D modeling, third dimensions effects that can be taken into account in 3D FEA are omitted, though the error between experimental results and RelNet model under loaded conditions are to be further analyzed.

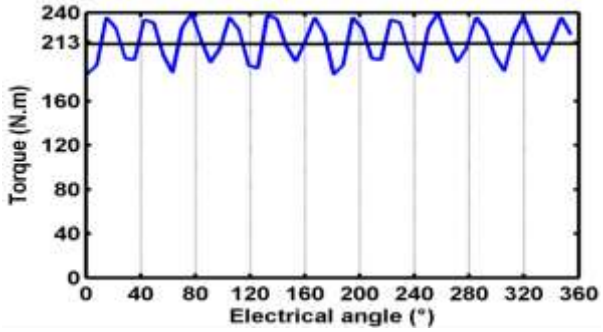

Fig. 21. RelNet torque ripple at 110 A rated current

V. Optimization Problem

For the proposed application, our aim is to find optimal physical characteristics of the axial flux machine with a view to minimize the machine's total losses on "Artemis automotive cycle" [8-15] and respect five non-linear constraints on the machine's Torques, Emf and Current density (J), as in (20).

$$\begin{cases} find\ X = [x_1, x_2, x_3, x_4, x_5, x_6] \\ \text{Minimize } E_{total} = E_{resist} + E_{iron} + E_{inverter} + E_{magnet} \\ \text{Under} \\ Emf_{bs} \le 200\,(\text{V}) \qquad Emf_{hs} \le 260\,(\text{V}) \\ \Gamma_{bs} = 100\,(\text{N.m}) \qquad \Gamma_{bs} = 33.3\,(\text{N.m}) \quad J \le 9\,(\text{A.mm}^{-2}) \end{cases} \tag{20}$$

The couples Torque-Speed issued from "Artemis road and urban cycles" are chosen in order to fit the Torque-Speed characteristic of the machine [15].

VI. Conclusion

In this paper a powerful tool for machine's design based on conventional reluctances network is presented. The modeling strategy is validated by means of 2D Finite Element and experimental results. When taking into account the non linearity a horizontal shift appears, this problem will be resolved in future work without compromising model computation time.

TABLE VI
Optimisation Results for Linear Models

Type	Description	Machine 6/4	Machine 6/8
Variables	Pole width	122.8 (mm)	69 (mm)
	Tooth width	96.8 (mm)	101.5 (mm)
	Magnet width	7.2 (mm)	9.2 (mm)
	Tooth height	40.9 (mm)	43.2 (mm)
	Rotor height	48.8 (mm)	33.39 (mm)
	Number of turns	12 (turns)	10 (turns)
Objective	Total losses	843.9 (KJ)	1067.5 (KJ)
Constraints	Basic speed Emf	151 (V)	116.8 (V)
	High speed Emf	260 (V)	260 (V)
	Current density	9 ($A.mm^{-2}$)	9 ($A.mm^{-2}$)
	Basic speed torque	100 (N.m)	100 (N.m)
	High speed torque	33.3 (N.m)	33.3 (N.m)

References

[1] J. Gyselinck, L. Vandevelde, and J.Melkebeek, "2D FE models, magnetic circuits and their coupling applied to the dynamic analysis of induction machines," in *Proc. 4th Int. Workshop Electr. Magn. Fields*, (EMF 1998), May, pp. 469–474.

[2] Z. Zhang, F. Profumo and A. Tenconi, "Axial-flux versus radial flux PM motors", *SPEEDAM*, 1996, Italy, pp. A4-19-25.

[3] K. Sitapati and R. Krishnan, "Performance comparison of radial and axial field permanent magnet brushless machines", *IEEE Transactions on Industry Applications*, Vol.37, No.5, Sept/Oct 2001, pp. 1219-1226.

[4] R. J. Hill-Cottingham, P. C. Coles, J. F. Eastham, F. Profumo, A.Tenconi and G. Gianolio, "Multi-disc axial flux stratosphericaircraft propeller drive", *IEEE Industry Applications Society Annual Meeting*, 2001.

[5] T. Raminosoa, I. Rasoanarivo, F. Meibody-Tabar, F.-M. Sargos, "Time-Stepping Simulation of Synchronous Reluctance Motors Using a Nonlinear Reluctance Network Method," IEEE Transactions on Magnetics, vol.44, no.12, pp.4618-4625, 2008.

[6] A. Delale, L. Albert, L. Gerbaud, F. Wurtz, "Automatic generation of sizing models for the optimization of electromagnetic devices using reluctance networks," IEEE Transactions on Magnetics, vol.40, no.2, pp. 830- 833, March 2004.

[7] H.W.Derbas, J.M.Williams, A.C. Koenig, S.D.Pekarek, "A Comparison of Nodal- and Mesh-Based Magnetic Equivalent Circuit Models," IEEE Transactions on Energy Conversion, vol.24, no.2, pp.388-396, 2009.

[8] G.Krebs, E.deCecco, C.Marchand, "Design approach of an axial flux motor for electrical powertrain vehicle," 2012, *ICEM*.

[9] M.L. Bash, J.M. Williams, S.D. Pekarek, "Incorporating Motion in Mesh-Based Magnetic Equivalent Circuits," IEEE Transactions on Energy Conversion, vol.25, no.2, pp. 329-338, 2010.

[10] B. du Peloux, L. Gerbaud, F. Wurtz, V. Leconte, F. Dorschner, " Automatic generation of sizing static models based on reluctance networks for the optimization of electromagnetic devices," IEEE Transactions on Magnetics, vol.42, no.4, pp. 715-718, 2006.

[11] D. Maquin, *Eléments de Théorie des Graphes.* Institut National Polytechnique de Lorraine, 2003.

[12] C. Espanet, "Modélisation et conception optimale de moteurs sans balais à structure inversée application au moteur-roue," Ph.D. dissertation, Franche-Comté Univ., Besançon, France, 1999.

[13] J. Pouget, " Conception robuste des machines asynchrones pour la traction ferroviaire," Ph.D. dissertation, Franche-Comté Univ., Besançon, France, 2009.

[14] M. Aydin, S. Huang; T.A. Lipo , "Design and 3D electromagnetic field analysis of non-slotted and slotted TORUS type axial flux surface mounted permanent magnet disc machines," in *Conf. Rec. 2001 IEEE Int. Conf. Electric Machines and Drives Conference*, pp.645,651.

[15] M.Hage Hassan, G.Remy, G. Krebs, C.Marchand, "Radial output space mapping for eletromechanical systems design, "2012, *OIPE*, pp.22-23